The Structure and Evolution of a Continental Winter Cyclone. Part II: Frontal Forcing of an Extreme Snow Event

JONATHAN E. MARTIN

Department of Atmospheric and Oceanic Sciences, University of Wisconsin—Madison, Madison, Wisconsin

(Manuscript received 5 September 1996, in final form 9 June 1997)

ABSTRACT

The production of a narrow, heavy, occasionally convective snowband that fell within a modest surface cyclone on 19 January 1995 is examined using gridded model output from a successful numerical simulation performed using the University of Wisconsin—Nonhydrostatic Modeling System. It is found that the snowband was produced by a thermally direct vertical circulation forced by significant lower-tropospheric warm frontogenesis in the presence of across-front effective static stability differences as measured in terms of the equivalent potential vorticity (PV_e). The sometimes convective nature of the snowband resulted from the development of freely convective motions forced by frontal lifting of the environmental stratification.

Model trajectories demonstrate that a stream of warm, moist air ascended through the trowal portion of the warm-occluded structure that developed during the cyclone life cycle. The lifting of air in the trowal was, in this case, forced by lower-tropospheric frontogenesis occurring in the warm-frontal portion of the warm occlusion. This trowal airstream accounts for the production of the so-called wrap-around precipitation often associated with occluded cyclones and, in this case, accounted for the northern third of the heavy snowband.

1. Introduction

Winter cyclones in the central United States are often accompanied by a variety of hazardous meteorological elements including strong winds, subfreezing temperatures, freezing rain, torrential rains, and heavy snow. The explosively deepening cyclones that occasionally visit this region are nearly always attended by some combination of these conditions (see, e.g., Schneider 1990; Marwitz and Toth 1993; Mass and Schultz 1993; Hakim et al. 1995). The much more common modest cyclones (i.e., modest as measured in terms of their minimum sea level pressure) can also be accompanied by dangerous weather. In fact, it is not uncommon for such ''garden variety'' winter cyclones to be attended by near-blizzard conditions and resulting heavy snowfalls (Moore and Blakely 1988; Shields et al. 1991; Hakim and Uccellini 1992; Funk et al. 1995; Shea and Przybylinski 1993).

Previous studies of snowbands in cyclonic storms have identified a number of processes responsible for the production of precipitation. Among these are jet streak interactions (Hakim and Uccellini 1992), frontogenesis in the presence of small moist symmetric stability (Sanders and Bosart 1985; Gyakum 1987; Moore and Blakely 1988), and large synoptic-scale lifting modified by local terrain effects (Dunn 1988). Conceptual understanding of the precipitation distribution in winter cyclones has also been distilled into a variety of forecasting ''rules of thumb.'' These include the likelihood that heavy snow will fall 200–250 km to the left of the track of the associated surface cyclone (NWSFO, Sullivan, Wisconsin). This region of a mature cyclone is often the occluded quadrant of the storm. It is not uncommon for experienced forecasters to refer to the heavy precipitation that often falls in this quadrant of the storm as ''wrap around'' precipitation. This term indicates that a portion of the cloud and precipitation shield has wrapped itself around to the west of the vortex center. It also, incorrectly, connotes that precipitation can be horizontally advected to different locations in a cyclone.

In the 1950s, scientists at the Canadian Meteorological Service developed a conceptual model for the structure of some North American cyclones that they termed the ''three front model'' (Godson 1951; Penner 1955; Galloway 1958, 1960). They found that this conceptual model was operationally very useful. A component of this conceptual model (devised by using frontal contour charts) was the trough of warm air aloft (trowal), which represented the axis of highest potential temperature θ ahead of the upper cold front in a warm-occluded cyclone. The trowal was shown to have a better correspondence to the sensible ''weather'' associated with a mature cyclone than was the surface

Corresponding author address: Dr. Jonathan E. Martin, Dept. of Atmospheric and Oceanic Sciences, University of Wisconsin—Madison, 1225 West Dayton St., Madison, WI 53706.
E-mail: jon@meteor.wisc.edu

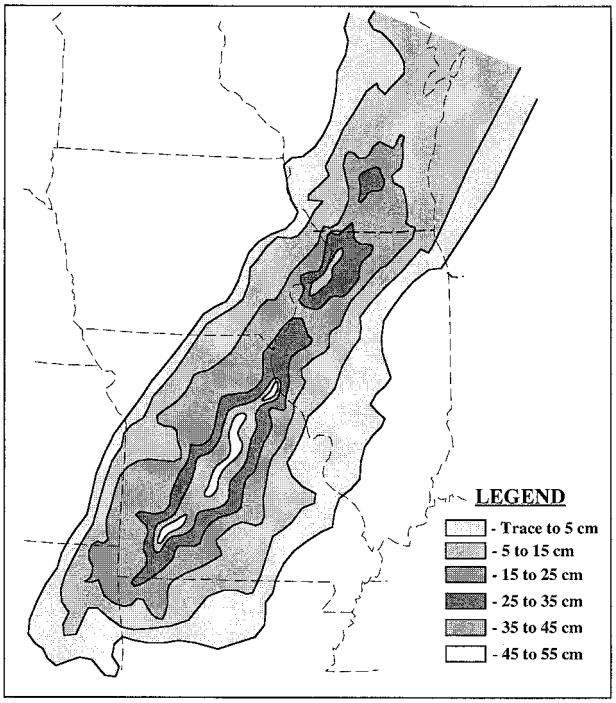

FIG. 1. Observed 24-h snowfall totals from 0000 UTC 19 January to 0000 UTC 20 January 1995. Totals are given in centimeters and are contoured every 10 cm except for the outermost contour, which represents trace amounts to 5 cm.

warm-occluded front (see Penner's Fig. 1). As a mature cyclone continues to develop, the trowal can be wrapped cyclonically around the cyclone center and can end up in the northwest quadrant of the decaying storm. The relationship between the trowal and heavy snowbands, although a reasonable and intriguing extension of prior work, has never been demonstrated in the literature.

In Part I (Martin 1998), the frontal structure and evolution of a modest cyclone that affected the central United States on 19 January 1995 was described. In the present paper the extreme snowfall event that accompanied this storm is examined. A finescale numerical model simulation of this cyclone is employed to describe the meso–synoptic-scale dynamic and thermodynamic circumstances that conspired to produce this record event. In section 2 observations of the snowband are presented. In section 3 we describe the numerical model used to simulate this case and verify the precipitation forecasts made by the model against the observations. Analysis of the mechanisms responsible for the production of the snowfall is presented in sections 4 and 5. This analysis will include extensive model-based air parcel trajectories, which will illustrate the airflow through the precipitation generation regions of the cyclone. We will discuss the results of this analysis in section 6 and offer conclusions in section 7.

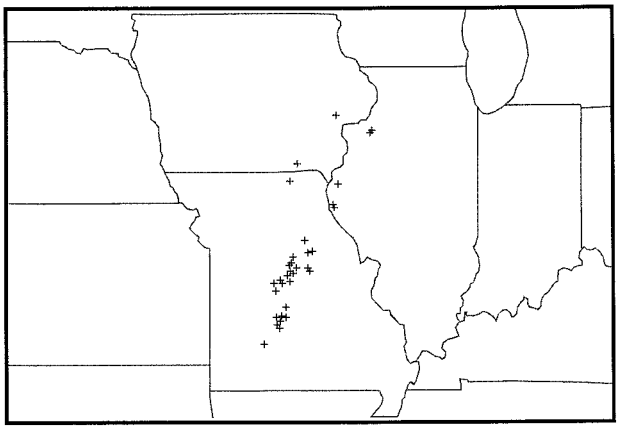

FIG. 2. Map of all cloud-to-ground lightning strikes associated with the snowband in the 24-h period 0000 UTC 19 January to 0000 UTC 20 January 1995. Crosses indicate positions of the lightning strikes.

2. Observations of the snowband

From 1800 UTC 18 January until 0600 UTC 20 January 1995 a modest surface cyclone affected the central United States. For a detailed description of the synoptic evolution of this cyclone and its attendant frontal structure, the reader is referred to Part I (Martin 1998). Despite the modest nature of the surface disturbance (its sea level pressure never fell below 997 hPa), this storm was attended by a band of heavy snow that stretched from Tulsa, Oklahoma, to north of Green Bay, Wisconsin (Fig. 1). Despite the synoptic-scale length of this band (nearly 1100 km), it was only a few hundred kilometers wide. In fact, the half-width of the snowband (defined as the lateral distance from the axis of maximum snowfall to a point receiving half the maximum amount) averaged only *63 km* along its entire length and was locally much narrower in central Missouri. Many locations affected by this precipitation feature received total snow accumulations from this single event that exceeded seasonal climatology.

An additional compelling characteristic of this snowband was its considerable convective nature, partial evidence for which is the density of cloud-to-ground lightning strikes associated with it (Fig. 2). Although snowfall accompanied by lightning is not an exceedingly anomalous occurrence in the central United States, the precise frequency of occurrence and the mean flash density of such events is unknown. In addition to the cloud-to-ground discharges shown in Fig. 2, in-cloud and cloud-to-cloud lightning was observed intermittently in southern Wisconsin between 1800 and 2200 UTC 19 January in association with this event (personal observation).

Central Missouri was hardest hit by the convective snowfall associated with this cyclone. At many locations the occasional thundersnow fell at rates exceeding 2″ (5 cm) per hour. As an example of the extremity of this event in central and southern Missouri a time series of

TABLE 1. Hourly time series of surface observations at Springfield, Missouri (SGF), from 2100 UTC 18 January to 2100 UTC 19 January 1995. Temperature T and dewpoint T_d are given in degrees Celsius, wind speed (SPD) is given in meters per second, wind direction (DIR) is given in degrees with 360° as north, sea level pressure (SLP) is given in hectopascals, R and S signify rain and snow, respectively, with the minus and plus indicating light and heavy intensities. OVC indicates overcast skies and X indicates obscured sky.

Time	T	T_d	DIR	SPD	SLP	COV	WX
2100	1°	0°	020	7.5	1012.6	OVC	R−
2200	1°	0°	020	7.0	1012.3	OVC	S−
2300	0°	−1°	020	9.0	1012.1	OVC	S
0000	0°	−1°	010	8.5	1011.8	OVC	S+
0100	0°	−1°	010	8.0	1011.8	X	S+
0200	−1°	−1°	020	8.5	1011.1	X	S+
0300	−1°	−2°	360	7.5	1011.1	X	S+
0400	−2°	−2°	360	8.0	1010.1	X	S+
0500	−2°	−2°	350	9.0	1009.7	X	S+
0600	−2°	−3°	360	8.0	1009.1	X	S+
0700	−2°	−2°	340	8.0	1007.9	X	S+
0800	−2°	−2°	340	8.5	1007.3	X	S+
0900	−2°	−2°	340	9.5	1006.6	X	S+
1000	−2°	−2°	340	9.5	1006.4	X	S+
1100	−2°	−2°	340	9.5	1006.5	X	S+
1200	−2°	−2°	330	10.0	1007.0	X	S+
1300	−1°	−2°	330	10.0	1008.1	X	S
1400	−1°	−2°	320	10.5	1009.0	X	S
1500	−1°	−1°	320	10.0	1009.3	X	S
1600	−1°	−1°	320	10.0	1010.6	OVC	S
1700	−1°	−1°	320	9.5	1011.3	OVC	S−
1800	0°	−1°	320	10.0	1011.5	OVC	S−
1900	1°	−1°	340	10.0	1011.4	OVC	S−
2000	2°	−1°	320	10.0	1011.7	OVC	S−
2100	2°	−2°	330	8.0	1012.4	OVC	

hourly observations from Springfield, Missouri (SGF), is shown in Table 1. From 0000 to 1200 UTC 19 January SGF reported 13 consecutive hours of heavy snow with nearly zero visibility and wind gusts topping 20 m s^{-1}. In the end, nearly 16″ (40 cm) of snow fell at Springfield. Columbia, Missouri, received a record 19.7″ (50 cm), which forced the closing of the University of Missouri for the first time in 17 years.

We now proceed to an analysis of the circumstances that conspired to produce this extreme snowfall event. This analysis will employ gridded output from a successful numerical simulation of this cyclone performed using the University of Wisconsin—Nonhydrostatic Modeling System (UW-NMS), which is described in the following section.

3. Numerical model simulation

To further elucidate the circumstances leading to the development of the snowband, output from a numerical forecast of this cyclone made using the University of Wisconsin—Nonhydrostatic Modeling System (UW-NMS) is used. UW-NMS is described by Tripoli (1992a,b). The model employs a two-way interactive, moveable nesting scheme, which allows for the simultaneous simulation of large synoptic-scale forcing as well as frontal-scale forcing. Prognostic variables carried by the model include u, v, w, and π (Exner function); ice–liquid potential temperature θ_{il}; and total water mixing ratio, as well as the mixing ratios for a variety of precipitation particles.

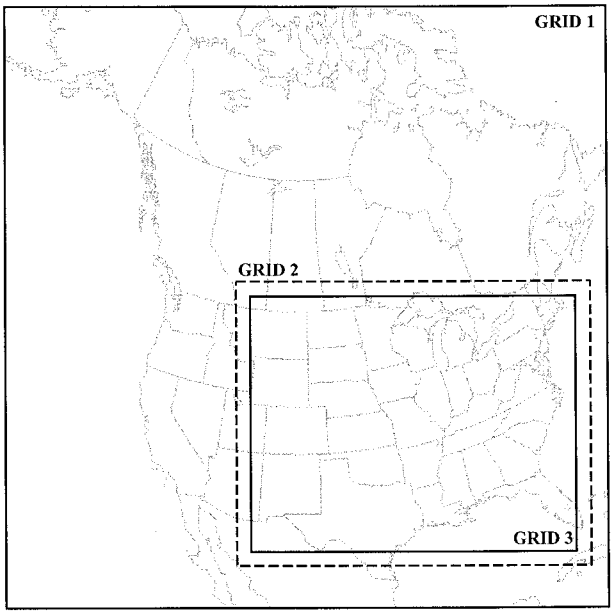

FIG. 3. Geographic locations of the three grids used in the numerical simulation described in the text.

Advection of the scalar variables is accomplished using a sixth-order Crowley scheme (Trembach et al. 1987), and the dynamic variables are advected using a second-order enstrophy-conserving leapfrog scheme (Sadourny 1975). Model physics include a radiation parameterization that predicts long- and shortwave radiative transfer in a cloudy atmosphere (Chen and Cotton 1983), and a predictive soil model with surface energy budget (Trembach and Kessler 1985). Liquid and ice processes are represented in the model by an explicit microphysics package that describes the evolution of cloud water, rainwater, pristine crystals, snow crystals, aggregate crystals, and graupel (Cotton et al. 1986; Flatau et al. 1989). A version of the Emanuel (1991) convective parameterization was employed, modified such that the convection equilibrates with the cyclone and frontal-scale vertical motion forcing (Tripoli 1996, personal communication). This modification reduces the sensitivity of the parameterization to the amount of convective available potential energy (CAPE) by tying the release of CAPE to the synoptic- and frontal-scale vertical motions.

Three grids were used in the simulation. Grid 1 (outer grid), grid 2 (middle grid), and grid 3 (inner grid) had horizontal resolutions of 160 km, 80 km, and 40 km, respectively. The data from grid 3 was used in this study. The geographic locations of these grids are shown in Fig 3.

The model employed geometric height as the vertical coordinate with discretely blocked out topography sim-

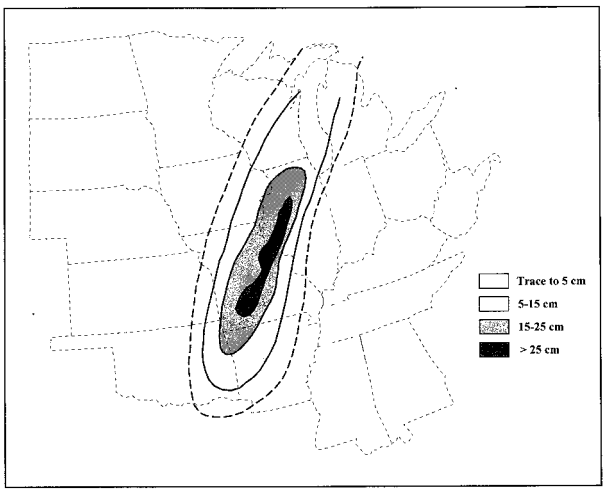

FIG. 4. UW-NMS model predicted snowfall totals from 0000 UTC 19 January to 0000 UTC 20 January 1995. Labeled and contoured as in Fig. 1.

ilar to that used in NCEP's Eta Model. Forty vertical levels were used with the vertical grid spacing of 200 m in the lowest five grid levels with a gradual geometric stretching (by a factor of 1.07) above such that the next 18 levels had an average spacing of 404 m and the top 17 levels had a spacing of 700 m. The model top was located at 19.2 km.

The model was initialized by interpolating directly from the 90.5-km NCEP Eta initialization, which has 50-hPa vertical resolution. Horizontal wind components, geopotential height, temperature, and relative humidity were interpolated horizontally along constant pressure surfaces to the locations of the model grid points. Data were then vertically interpolated to the model grid levels. The lateral boundaries were updated every 6 h from the Eta gridded forecasts using a Rayleigh-type absorbing layer. The simulation was initialized at 0000 UTC 19 January 1995 and was run for 48 h. Only the first 36 h of this two-day run are used in this study. Air parcel trajectories were calculated using u, v, and w from the model output, using a forward differencing scheme with a time step of 24.5 min.

A systematic verification of the model simulation will not be presented here. The reader is referred to Martin (1998) for comparisons between the simulation and the actual observations. As further evidence of the accuracy of this simulation, we present in Fig. 4 the snowfall total map from the UW-NMS simulation. A gratifying similarity exists between Figs. 1 and 4 testifying to the fidelity of the simulation. Although exact agreement does not exist between the observations and the simulation (most notably, the model snowfall totals, although considerable, are not as extreme as the observed totals) the horizontal dimensions of the band were quite accurately simulated. Such agreement on the precipitation distribution suggests that the mesoscale dynamical forcing of the snowband was also accurately replicated in the model data. As a result, the gridded output from this simulation will be used to describe the mesosynoptic environment in which the record snowfall that characterized this cyclone developed.

4. Forcing of the snowband

As noted in the previous section, the snowband that accompanied this modest cyclone was noteworthy for a number of reasons: 1) the snowfall totals were exceptional for the region, 2) the band was characterized by intermittent convection throughout most of its life history, and 3) the band had synoptic-scale length ($\sim$1100 km) but mesobeta-scale width (especially in terms of its half-width). In this section and the next, a diagnosis of the dynamic and thermodynamic circumstances that led to the development and aforementioned characteristics of the snowband will be presented. This diagnosis will center on the role of frontogenesis in generating the requisite vertical motion for precipitation generation. In the following subsection, frontogenesis and its relation to the forcing of vertical circulations is reviewed.

a. Frontogenesis and vertical circulations

Frontogenesis is the time rate of change of the magnitude of the potential temperature gradient (Petterssen 1936). By virtue of the wavelike structure of midlatitude cyclones, the horizontal flow associated with them almost always contains significant deformation. Elegant theoretical work by Sawyer (1956) and Eliassen (1962) has shown that differential thermal advection in a horizontal deformation field can lead to a thermally direct vertical circulation by increasing the magnitude of the horizontal temperature gradient and inducing accelerations in the direction of the thermal wind vector. Such differential thermal advection can increase $|\nabla\theta|$ (i.e., it can be frontogenetic). Therefore, wherever the horizontal flow acts to concentrate the horizontal potential temperature gradient, a thermally direct vertical circulation will likely develop. A 2D version of the Miller (1948) frontogenesis function

$$F_{2D} = \frac{d}{dt}|\nabla\theta| = \frac{1}{|\nabla\theta|}\left[-\frac{\partial\theta}{\partial x}\left(\frac{\partial u}{\partial x}\frac{\partial\theta}{\partial x}+\frac{\partial v}{\partial x}\frac{\partial\theta}{\partial y}\right)-\frac{\partial\theta}{\partial y}\left(\frac{\partial u}{\partial y}\frac{\partial\theta}{\partial x}+\frac{\partial v}{\partial y}\frac{\partial\theta}{\partial y}\right)\right] \quad (1)$$

represents the contribution to frontogenesis from the horizontal deformation. Here, the total derivative is

$$\frac{d}{dt} = \frac{\partial}{\partial t} + u\frac{\partial}{\partial x} + v\frac{\partial}{\partial y}. \quad (2)$$

Calculations of frontogenesis in this paper are made using (1) employing the total horizontal winds and po-

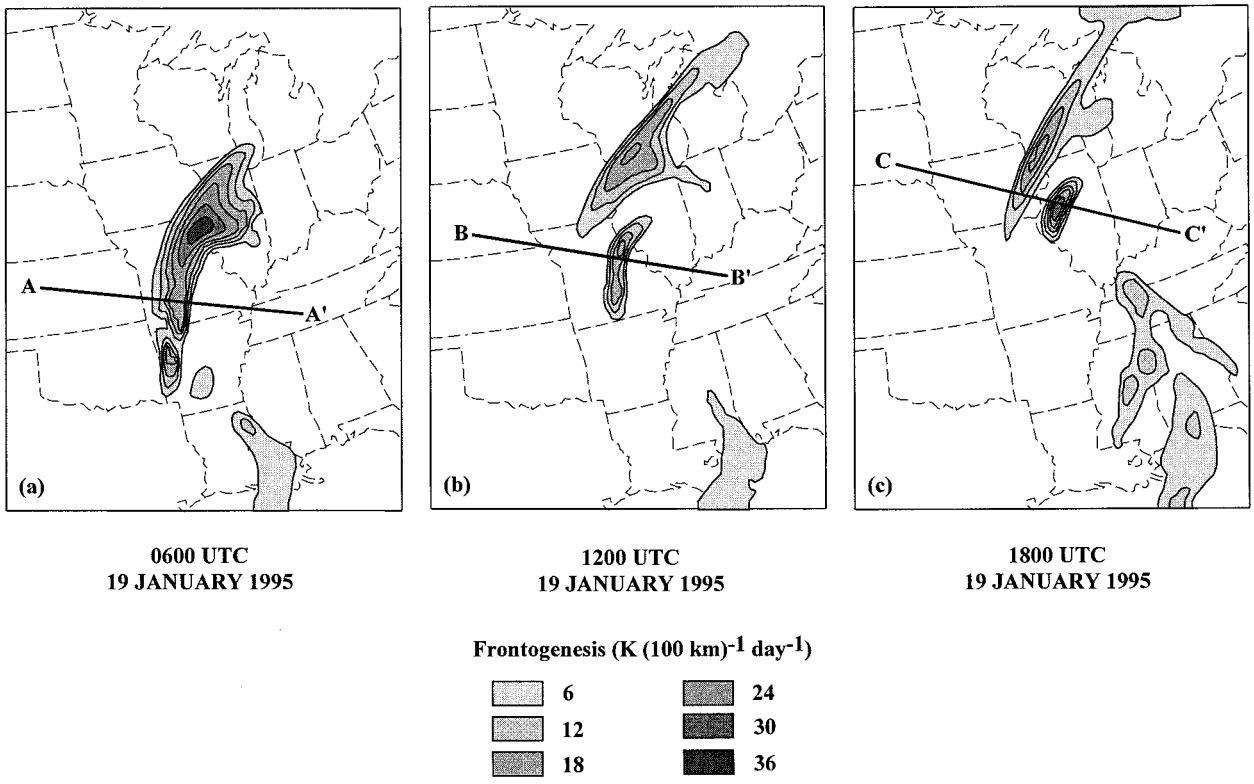

FIG. 5. Two-dimensional frontogenesis function at 1.96 km at (a) 0600 UTC 19 January, (b) 1200 UTC 19 January, and (c) 1800 UTC 19 January 1995. Frontogenesis [K (100 km)$^{-1}$ day^{-1}] is labeled and contoured every 6 K (100 km)$^{-1}$ day^{-1} beginning at 6 K (100 km)$^{-1}$ day^{-1}. Cross sections along AA' in (a) are shown in Fig. 8; along BB' in (b) are shown in Fig. 11; and along CC' in (c) are shown in Fig. 12.

tential temperatures from the 40-km simulation of this case. Although (1) ignores the modifying effect of vertical velocity on gradient strength, it more clearly reveals the region and circumstances for the forcing of vertical circulations (especially in the middle troposphere) than does the traditional Miller (1948) frontogenesis function. It should be noted that when the total winds are replaced by the geostrophic winds in (1) and (2), the quasigeostrophic frontogenesis function [which involves the **Q** vector (Hoskins et al. 1978)] is returned.

Shown in Fig. 5 is a series of 6-h plots of frontogenesis at 1.96 km from the UW-NMS model simulation. Although representing only one horizontal level, Fig. 5 demonstrates that the axis of maximum lower-tropospheric frontogenesis was consistently coincident with the position of the snowband. In subsequent sections of the paper, more detailed analysis at each of the indicated times is presented in order to more fully explain the production of this snowband. This analysis begins at 0600 UTC 19 January 1995.

b. 0600 UTC 19 January 1995

Moderate to heavy snow was falling over much of central and southwest Missouri at 0600 UTC 19 January. Between 0600 and 0700 UTC, a total of 10 cloud-to-ground lightning strikes were recorded in association with the snowfall. Doppler radar reflectivity from Kansas City, Missouri (MCI), at 0647 UTC 19 January is shown in Fig. 6. There were two rather distinct bands of precipitation in central Missouri at this time. Band 2 was the most intense band with reflectivities in the 35–40-dBZ range, uncommon for snowfall. Band 1 was further from the radar and beam attenuation may have disguised its vigor. It was certainly convective in nature as it was associated with cloud-to-ground lightning at 0647 UTC. Both bands were approximately 35 km wide and there was a spacing of roughly 35 km between them.

Also portrayed in Fig. 6 are the mean isentropes in the 2–5-km layer as forecasted by the UW-NMS model. Thus, the snowbands depicted by the radar were oriented nearly parallel to the 2–5-km thermal wind vector at this time. Such a circumstance suggests that a mesoscale frontal instability, such as conditional symmetric instability (CSI), may have been acting to organize the precipitation bands.

CSI is a 2D, semigeostrophic mesoscale instability in which both gravitational and inertial buoyancy determine the displacement of an air parcel (Bennetts and Hoskins 1979; Emanuel 1983). Assuming no variation in the along-shear (front) direction, the vertical and horizontal accelerations of a saturated parcel of air are given, respectively, by

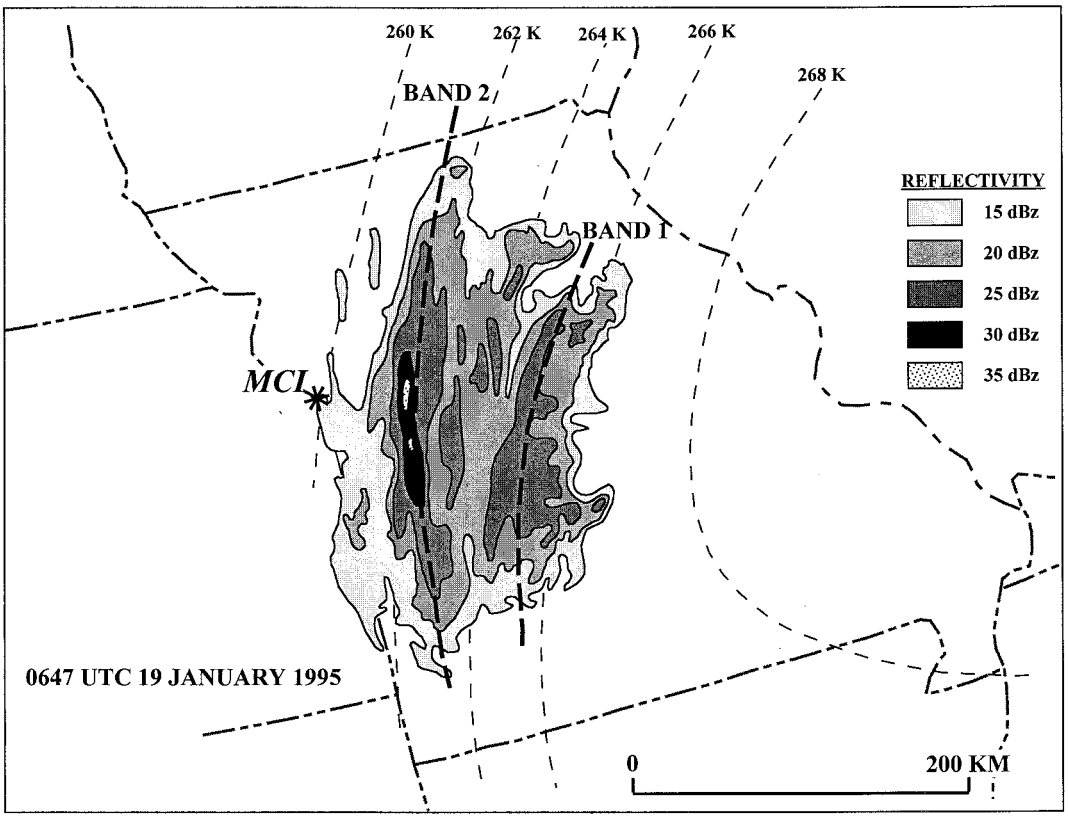

FIG. 6. WSR-88D radar reflectivity at 0647 UTC 19 January 1995 from Kansas City, Missouri (MCI). Reflectivity (dBZ) is labeled and contoured every 5 dBZ beginning at 15 dBZ. Thin dashed lines are 2–5-km mean layer isentropes at 0600 UTC calculated from the UW-NMS simulation. Heavy dashed lines indicate distinct bands designated band 1 and band 2.

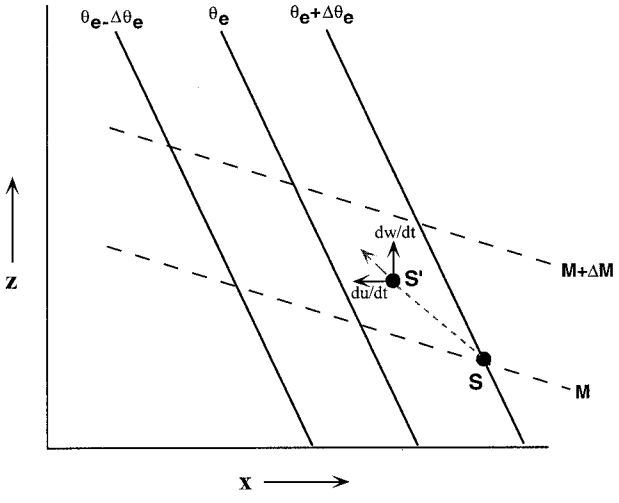

FIG. 7. Schematic vertical cross section depicting an environment susceptible to release of CSI. Solid lines are isopleths of θ_e. Dashed lines are isopleths of M. A saturated parcel displaced along slanted path SS' will experience the indicated component and resultant accelerations as described in the text.

$$\frac{dw}{dt} \propto (\theta_{eP} - \theta_{eE})$$

$$\frac{du}{dt} \propto (M_P - M_E). \tag{3}$$

Here, M is the geostrophic pseudoabsolute momentum defined as

$$M = V_g + fx, \tag{4}$$

where f is the Coriolis parameter and x is positive in the across-shear direction toward warm air. The subscripts P and E refer to parcel and environmental values, respectively.

Figure 7 shows a schematic cross section through an environment susceptible to CSI. In such an environment, a saturated parcel displaced along the slanted path SS' would continue to accelerate in that direction. As shown in Fig. 7, the necessary condition for CSI is that the isopleths of θ_e are more steeply sloped than the isopleths of M. Bennetts and Hoskins (1979), Emanuel (1983), Shields et al. (1991), and Martin et al. (1992) noted that for 2D flow this condition is identical to the equivalent potential vorticity (PV_e) being negative. Moore and Lambert (1993) and McCann (1995) extended this idea

by performing analyses of PV_e and noting its utility in delineating regions susceptible to CSI. Finally, it should be noted that an environment that is stable to purely vertical and purely horizontal displacement (as in the schematic in Fig. 7) may still be unstable to slantwise displacement.

Thorpe and Emanuel (1985) performed a modeling study that physically explained why an environment characterized by CSI may be important in the generation of precipitation bands. They showed that the circulation produced by a given frontogenetic forcing is sensitive to across-front differences in the slantwise stability—a fact implicit in the determinant of the Sawyer–Eliassen circulation equation. When the slantwise stability is lower on the warm, saturated side of the front (i.e., when the PV_e is lower on the warm side), an intense, horizontally restricted updraft occurs in that air mass while a gentle, widespread downdraft occurs in the colder, drier air behind the front. This is because the PV_e, being a measure of the effective static stability, plays an analogous role in the Sawyer–Eliassen equation to that played by static stability in the quasigeostrophic omega equation; where the PV_e is small, the response to frontogenetic forcing is large, and vice versa. In order for mass balance to be maintained across the front, the vigorous updraft must be horizontally restricted, leading to its manifestation as a thin, banded precipitation feature. Many studies have suggested that the production of banded precipitation in cyclonic storms results from this combination of frontogenetic forcing and an environment susceptible to release of CSI as determined by the slope of M and θ_e lines (see, e.g., Sanders and Bosart 1985; Sanders 1986; Moore and Blakely 1988; Martin et al. 1992). It is important to note that only the across-front *difference* in the effective static stability is necessary to produce narrow bands of precipitation in frontal regions.

In recent numerical simulations of unforced, hydrostatic, nonlinear CSI, Persson and Warner (1993) found that explicit resolution of CSI circulations could not be achieved at horizontal grid spacings coarser than 30 km. The current study, therefore, cannot offer evidence for the occurrence or nonoccurrence of CSI circulations, or of the structures produced by such circulations, in this case. Instead, in the following analyses the model output will be used to determine whether or not the necessary condition for CSI, referred to earlier, was found in the frontal environment of this cyclone. Figure 8 presents cross sections along line AA' in Fig. 5. Shown in Fig. 8a is the model-derived M and θ_e analyses at 0600 UTC 19 January. The shaded regions were subjectively determined to be susceptible to CSI by the conventional method of evaluating slopes of M and θ_e isopleths. Considerable portions of the entire shaded area are simply regions of potential instability (i.e., $\partial\theta_e/\partial z < 0$), a special case of CSI. The rather limited region of pure CSI (the darker area in Fig. 8a) was located in the 5–8-km layer. Although between 5 and 6 km this air was subject to considerable lifting, the relative humidities were, at best, about 80% (Fig. 8d). Since release of CSI requires the air to be saturated, this elevated region of CSI was likely not released at this time. Importantly, however, the PV_e along the same cross section (Fig. 8b) demonstrates that, in the nearly 2D environment of the warm front, negative values of PV_e occur in a similar region as the shaded areas of instability portrayed in Fig. 8a. This circumstance will now be related to the observed narrowness of the band. The cross section of θ_e in Fig. 8b demonstrates the presence of a deep moist neutral/potentially unstable layer on the warm side of the front. The 2D frontogenesis along AA' is shown in Fig. 8c. A deep layer of substantial frontogenesis was associated with the warm front at this time. An interesting feature in Fig. 8c is the two regions of negative PV_e that straddle the frontogenesis axis. For PV_e to be a reliable measure of the effective static stability of air parcels, the air must be saturated. This condition was met only on the warm side of the front. As a consequence, there was considerably less resistance to vertical displacement on that side of the front. Thus, theory predicts the presence of an intense, more horizontally restricted updraft on the warm side and a considerably less noticeable downdraft on the cold side. The vertical motion from the model provides exactly that distribution (Fig. 8d) although it is not detailed enough to resolve the multiple banded structure observed in Fig. 6. Thus, it is likely that the narrow across-front dimension of the snowband resulted from across-front differences in the effective static stability (as measured in terms of PV_e) in the presence of a thermally direct frontogenetic circulation. Although the absence of saturated regions of CSI in the frontal environment of the simulation seems to suggest that release of CSI was not a factor in the production of the banded structure shown in Fig. 6, the model resolution used in this study precludes making a definitive statement regarding the role of release of CSI.

The circumstances that forced the width of the snowband do not necessarily explain its convective nature at 0600 UTC. A combination of model trajectories and real sounding data are now used to explain the development of the convective snow.

c. Production of convective snow at approximately 0600 UTC

Figure 9 is a plan view of trajectories, located within the maximum updraft region along line AA' at 0600 UTC, traced backward to their origins at 0000 UTC 19 January. Fortuitously, these parcels originated within 25 km of the real sounding site at Little Rock, Arkansas (LZK). In this section, these three parcels will be investigated in an attempt to diagnose the development of the convective snowfall in central Missouri at about 0600 UTC. Parcel 1, originally located at 869 hPa, was lifted to 621 hPa between 0000 and 0600 UTC. Parcel 2 rose from 801 to 599 hPa and parcel 3 from 729 to

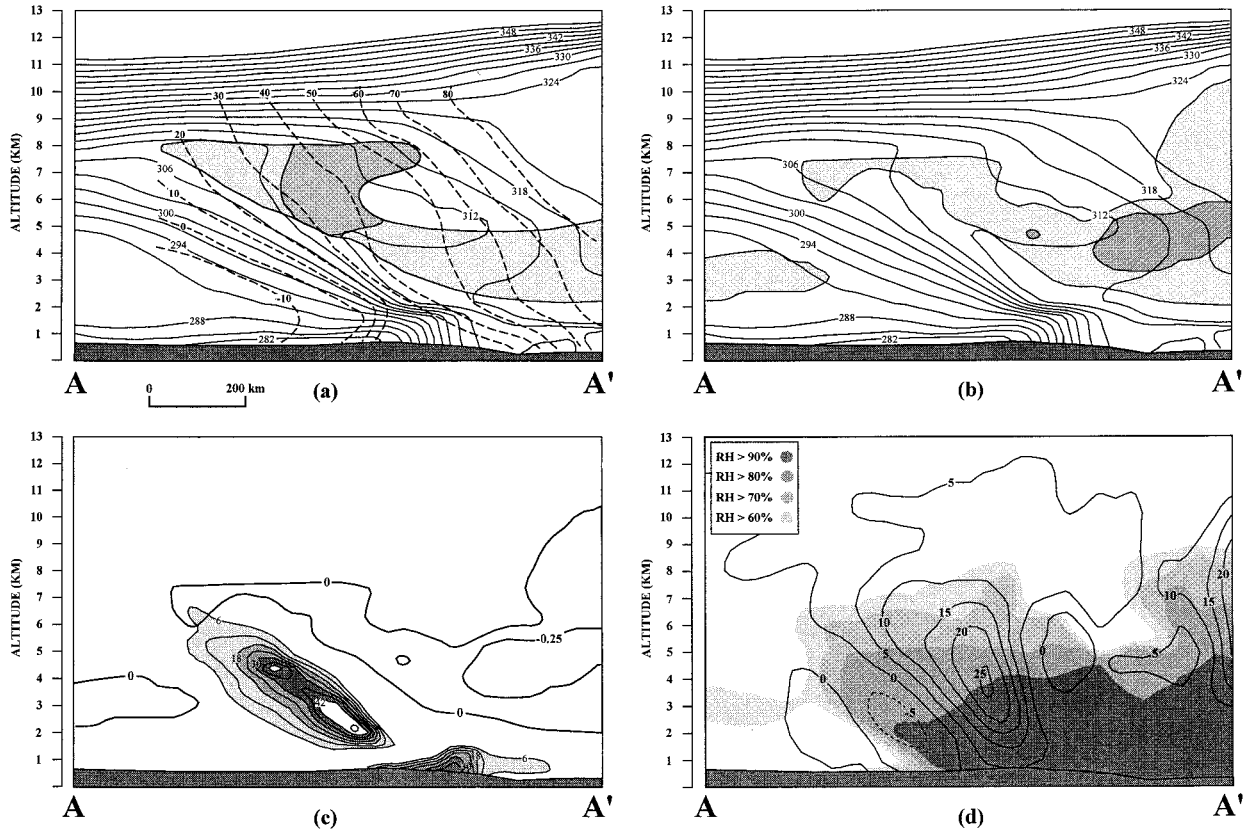

FIG. 8. (a) Cross section, along AA' in Fig. 5a, of M and θ_e from the UW-NMS simulation at 0600 UTC 19 January 1995. Solid lines are isentropes of θ_e (K), labeled and contoured every 3 K. Dashed lines are isopleths of M (m s^{-1}) labeled and contoured every 10 m s^{-1}. Shaded area was subjectively determined to be susceptible to CSI. Darkest shaded area represents area susceptible to pure CSI, lighter shaded area represents area of potential instability. (b) Cross section, along AA' in Fig. 5a, of PV_e and θ_e at 0600 UTC 19 January 1995. Isentropes of θ_e labeled and contoured as in Fig. 8a. Shaded area has negative PV_e; light shading shows values from 0 to -0.25 PVU (1 PVU $= 10^{-6}$ m^2 s^{-1} K kg^{-1}), darker shading shows values of -0.25 to -0.50 PVU. (c) Cross section, along AA' in Fig. 5a, of 2D frontogenesis [K (100 km)$^{-1}$ day^{-1}] at 0600 UTC 19 January 1995 labeled and contoured every 6 K (100 km)$^{-1}$ day^{-1}. Thicker solid lines outline regions of negative PV_e depicted in Fig. 8b. (d) Cross section, along AA' in Fig. 5a, of vertical motion (cm s^{-1}) labeled and contoured every 5 cm s^{-1}. Solid lines are upward vertical motions and dashed lines are downward vertical motions. Shading shows model relative humidity (RH), labeled in percent and shaded every 10% from greater than 60% to greater than 90% with legend in top left.

632 hPa during that same time interval. These parcel displacements are taken directly from the trajectory analyses.

The model-derived sounding at the origin of the trajectories is shown in Fig. 10a. The relative humidity gradually diminishes from near 100% at the surface to considerably lower values in the middle troposphere. The actual LZK sounding at 0000 UTC 19 January is shown in Fig. 10b. Since LZK was located in the warm sector, where horizontal variations of temperature and dewpoint are minimal, its stratification was representative of the stratification along the entire trajectory paths shown in Fig. 9. With the exception of a weaker low-level inversion, the model initialized sounding fairly well represents the lower-tropospheric vertical temperature profile present in the observations. However, in the 900–800-hPa layer, slightly smaller values of relative humidity in the model sounding have important consequences for the diagnosis of the convective activity as the model underestimates the potential instability in that layer. The implications of these subtle differences between model and observed soundings were examined by applying the model net vertical displacements to both the model and observed soundings for the chosen parcels. For instance, upon lifting parcel 1 assuming the model sounding, a state of deep neutrality is achieved. Lifting parcel 2 against the model sounding creates a meager amount of free convection in a shallow layer. Parcel 3 remains negatively buoyant when lifted against the model sounding.

When lifting these parcels against the observed stratification, the seemingly slight difference between the model and observed soundings at 800-hPa renders parcel 2 freely convective upon being lifted to 730 hPa (easily achieved by that parcel). Thus, when air motions described by the model are made to lift the observed environmental stratification, free convection is easily achieved at approximately 0600 UTC in the correct ob-

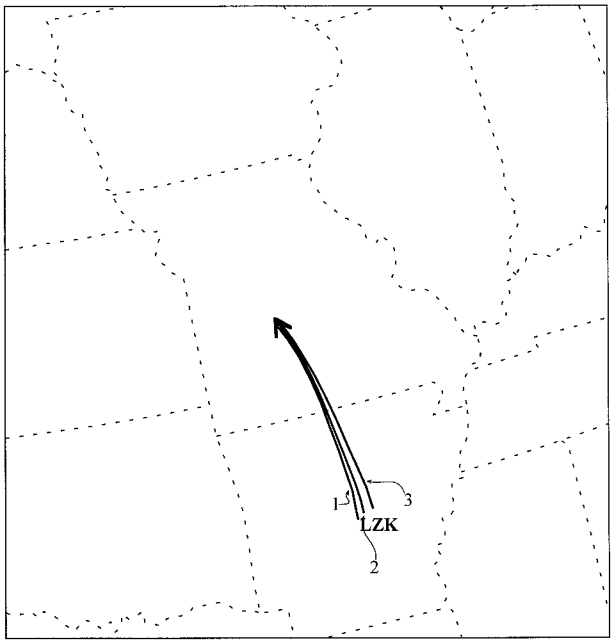

FIG. 9. The 6-h absolute trajectories of parcels located in the maximum updraft region of Fig. 8d at 0600 UTC traced backward to 0000 UTC 19 January 1995. Location of Little Rock, Arkansas (LZK), is indicated.

served location. Discretized models cannot avoid vertical smearing of information. The vertical smearing of thermodynamic variables, particularly moisture variables, which can exhibit enormous gradients in the vertical, can be of great consequence in any study that aims to diagnose moist convective processes. The inability of the model sounding to produce the observed convection, itself a result of the model's inability to replicate (or even initialize) existing vertical gradients in moisture, may well have been a contributing factor in its underestimate of snowfall totals, which were particularly erroneous in central Missouri.

d. 1200 UTC 19 January 1995

By 1200 UTC moderate to heavy snow continued in central Missouri while light to moderate snow had invaded eastern Iowa and northwestern Illinois. The main snowband was still oriented parallel to the 2–5-km mean isentropes (not shown) and so a similar set of circumstances, conducive to the forcing of a narrow updraft, existed at 1200 UTC 19 January. For reference, the 2D frontogenesis function at 1.96 km at that time is shown in Fig. 5b. A noticeable decrease in the intensity of the frontogenesis had occurred by this time as separate maxima developed. A series of vertical cross sections along line *BB′* in Fig. 5b are shown in Fig. 11.

To determine whether or not the environment was susceptible to release of CSI, a cross section of model-

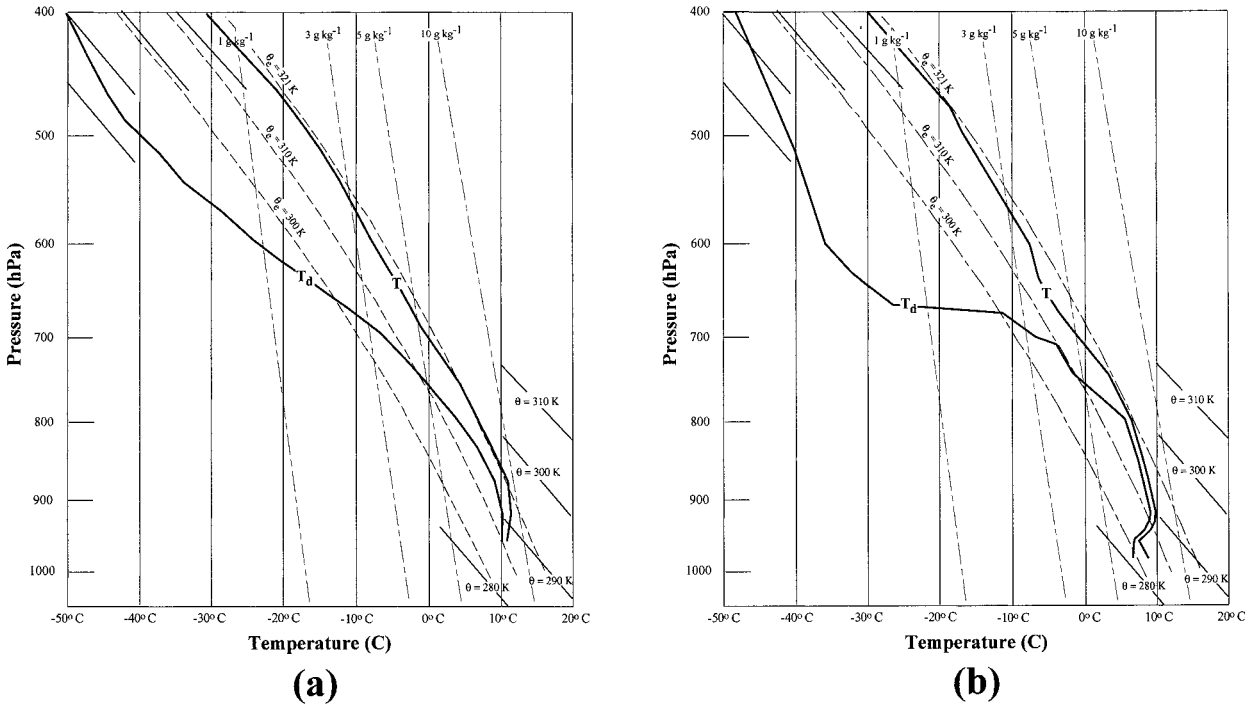

FIG. 10. (a) Pseudoadiabatic diagram depicting the UW-NMS model initialized sounding at 0000 UTC 19 January 1995 at the origin of trajectories shown in Fig. 9. Temperature and dewpoint soundings are indicated by T and T_d, respectively. (b) As in Fig. 10a except observed Little Rock, Arkansas (LZK), sounding at 0000 UTC 19 January 1995.

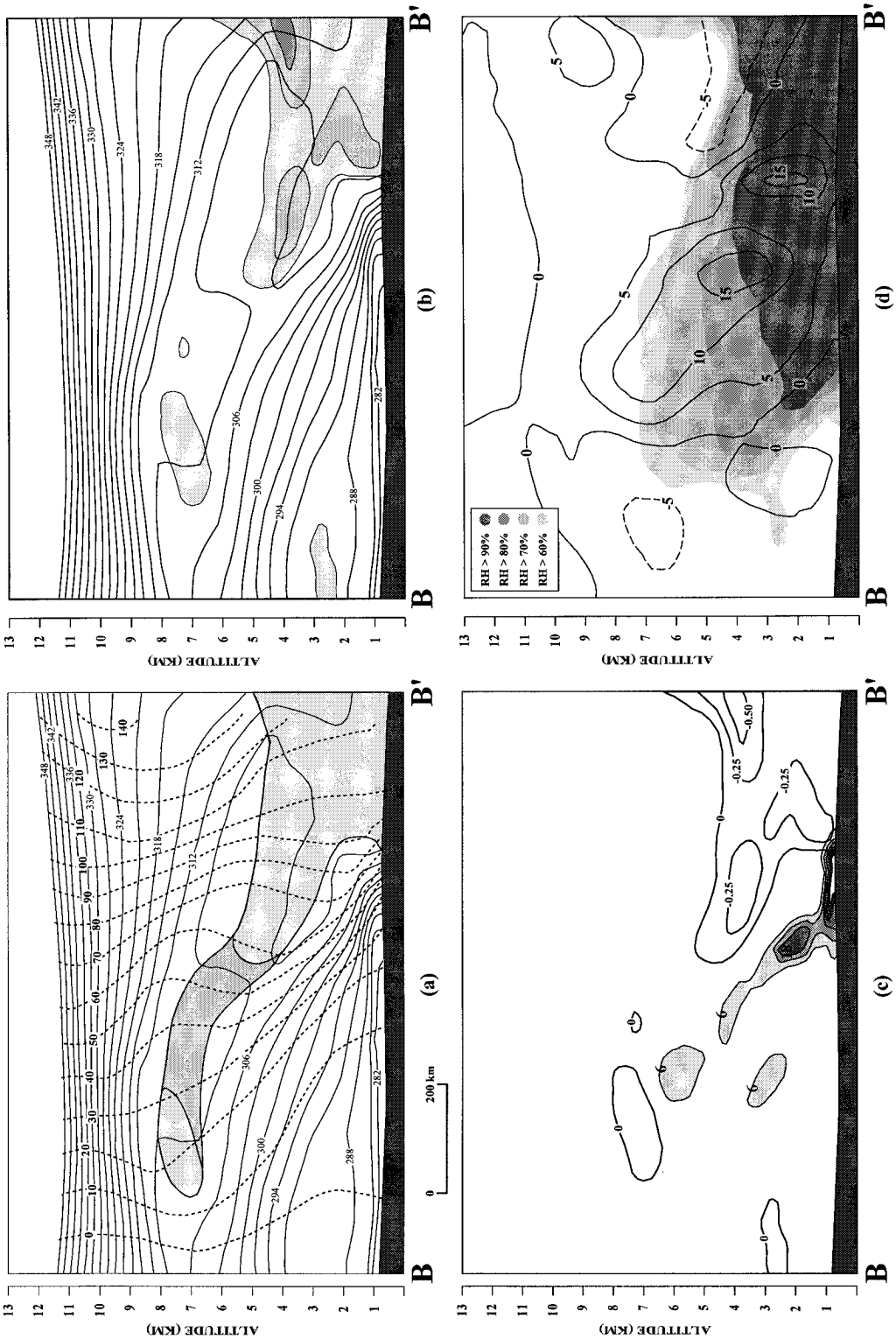

FIG. 11. (a) As in Fig. 8a except along line *BB′* in Fig. 5b at 1200 UTC 19 January 1995. (b) As in Fig. 8b except along line *BB′* in Fig. 5b at 1200 UTC 19 January 1995. (c) As in Fig. 8c except along line *BB′* in Fig. 5b at 1200 UTC 19 January 1995. (d) As in Fig. 8d except along line *BB′* in Fig. 5b at 1200 UTC 19 January 1995. Darkest shading represents PV_e values from −0.50 to −0.75 PVU.

derived M and θ_e at 1200 UTC is shown in Fig. 11a. As was the case at 0600 UTC, the subjectively determined area susceptible to release of CSI (shaded) was almost entirely a region of potential instability. Only a small, upper-level, unsaturated portion of the shaded area was characterized by true CSI. The area of negative values of PV_e for the same cross section is shown in Fig. 11b. The near equivalence of the two regions demonstrates the power and precision of using PV_e as a gauge of effective static stability.

The 2D frontogenesis function is shown in Fig. 11c. As suggested in Fig. 5b, the intensity of the frontogenesis had decreased noticeably by this time. In the presence of the across-front static stability differences that existed at this time, even this rather modest frontogenesis was able to produce a significant, narrow updraft (in the 1–3-km layer) as shown in Fig. 11d. The axis of the updraft maxima throughout the lower troposphere is slanted upward along the frontal surface.

The above analysis suggests that, as before, the unsaturated regions of pure CSI in the model simulation were probably not involved in the production of the snowband. Instead, frontogenesis in the presence of across-front effective static stability differences (manifested almost entirely in potential instability) resulted in the dimensions and intensity of the snowband. As had been the case at 0600 UTC, at 1200 UTC the model was not able to resolve the observed convection and thus could not produce accurate snowfall amounts.

e. 1800 UTC 19 January 1995

At 1800 UTC moderate to heavy snow was occurring from Columbia, Missouri, to Dubuque, Iowa. The snowband remained parallel to the midlevel thermal wind (not shown) as had been the case at prior times. Recall that the 2D frontogenesis function at 1.96 km at 1800 UTC is shown in Fig. 5c. The intensity of the frontogenesis was slightly greater than it had been 6 h earlier and was again nearly coincident with the axis of heaviest snow. A series of vertical cross sections along line CC' in Fig. 5c are shown in Fig. 12.

As was the case at previous times, regions of negative PV_e locate regions susceptible to CSI (Fig. 12a). Once again, only the uppermost, unsaturated portion of this region was true CSI (not shown). A hint of the midlevel warm-occluded structure that began to form around this time can be seen in the isopleths of θ_e (Fig. 12a). A description of the development of this structure is given in Martin (1998). The 2D frontogenesis function along CC' is shown in Fig. 12b. The depth and magnitude of the frontogenesis remained modest at 1800 UTC but in the presence of the notable across-front difference in effective static stability even this modest frontogenesis was enough to generate a narrow, vigorous updraft above 2 km (Fig. 12c).

Although the cloud-to-ground lightning data did not indicate any discharges after 1510 UTC, there were in-cloud and cloud-to-cloud discharges observed in southern Wisconsin between 1800 and 2200 UTC (personal observations). These observations, combined with the intensity of the snowfall, suggested a convective component to the precipitation was occurring at this time. A series of four parcels, located near the maximum updraft along CC' at 1800 UTC, were traced backward to 1200 UTC to determine what influence the environmental static stability had on the generation of the convective snowfall at 1800 UTC.

Figure 13 shows that the four parcels located along CC' at 1800 UTC originated less than 80 km to the northwest of Paducah, Kentucky (PAH), at 1200 UTC. Thus, the PAH sounding at 1200 UTC (which was located in the warm sector at this time) was used to describe the stratification of the actual air that was lifted as it moved along the trajectory path indicated in Fig. 13. Shown in Fig. 14 is the actual 1200 UTC sounding from PAH along with the model-forecasted sounding at that site at 1200 UTC. The most obvious difference between these two soundings is in the rate at which drying occurs above the moist layer. The actual sounding (Fig. 14b) indicates that the moist layer extended up to 735 hPa and was abruptly capped by an extremely dry layer. In fact, it should be noted that the sounding presented in Fig. 14b is actually modified from the radiosonde data as the extreme drying encountered by the sonde resulted in evaporative cooling and the production of spurious layers of superadiabatic lapse rates atop the moist layer. The model sounding (Fig. 14a) begins drying out at 785 hPa and the drying is spread over a 50-hPa layer. As a result, the extreme vertical gradients of θ_e that actually existed in nature were not captured in the model and it underestimated the degree of potential instability at midlevels. The consequences of this fact are now discussed.

Parcel 1 in Fig. 13 rose from 796 to 591 hPa (1.87 to 4.16 km) during the 6-h interval from 1200 to 1800 UTC. When this amount of lifting (in the same layer) is applied to the actual 1200 UTC sounding at PAH, the parcel becomes freely convective at 685 hPa and positive area exists from that level up to 610 hPa. The same lifting applied to the model's 1200 UTC sounding does not result in free convection. In fact, the model parcel remains negatively buoyant throughout the period. A similar set of circumstances applied to the other three parcels in this analysis. Parcel 2 [which rose from 844 to 622 hPa (1.39 to 3.18 km)] became freely convective at 710 hPa with positive area extending up to 580 hPa when the lifting was applied to the real sounding. Lifted against the model sounding, parcel 2 remains negatively buoyant throughout the ascent. Parcel 3 [which rose from 864 to 653 hPa (1.2 to 3.4 km)] also generated positive area in the real sounding from 715 to 590 hPa but slight negative buoyancy in the model sounding. Parcel 4, which originated at 750 hPa, became freely convective at 715 hPa in the real sounding and did so with mixing

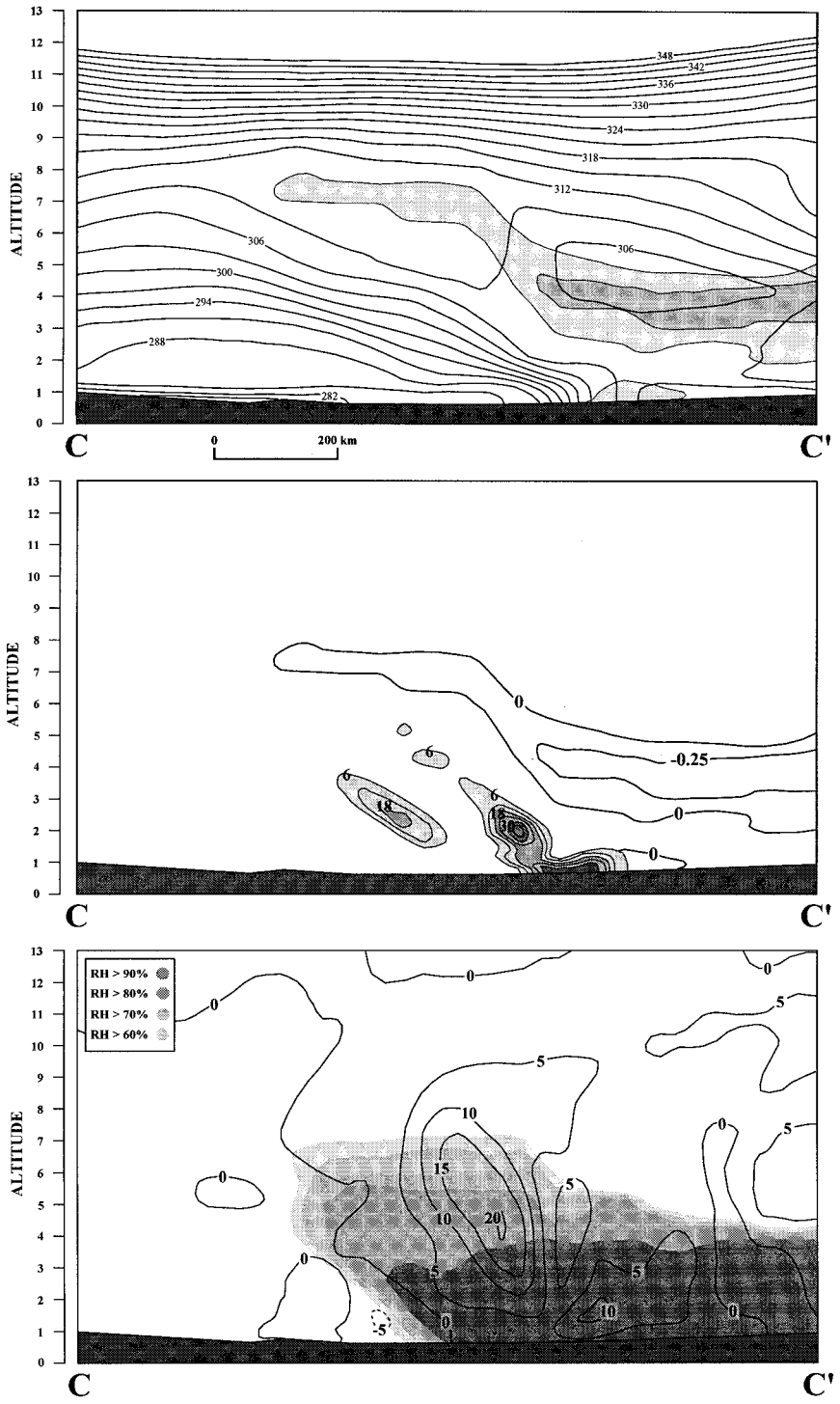

FIG. 12. (a) As in Fig. 8b except along line *CC′* in Fig. 5c at 1800 UTC 19 January 1995. (b) As in Fig. 8c except along line *CC′* in Fig. 5c at 1800 UTC 19 January 1995. (c) As in Fig. 8d except along line *CC′* in Fig. 5c at 1800 UTC 19 January 1995.

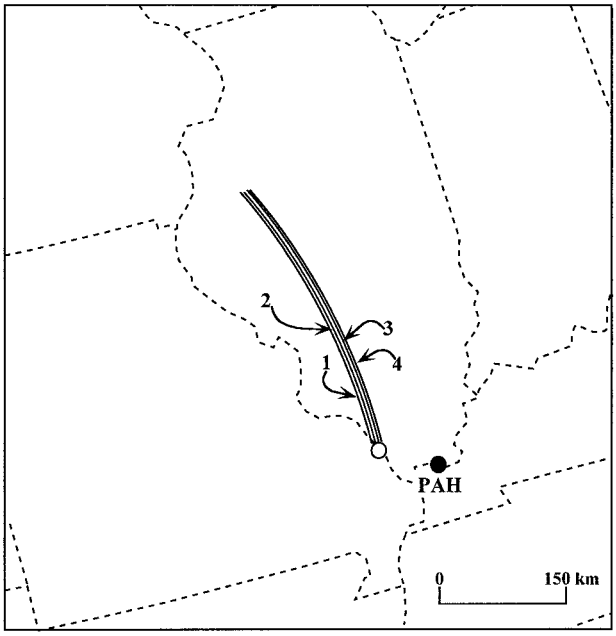

FIG. 13. The 6-h absolute trajectories from 1200 to 1800 UTC 19 January 1995 beginning at the unshaded circle. Parcels 1, 2, 3, and 4 are referred to in the text. Location of Paducah, Kentucky (PAH), is indicated.

ratios in the 4–4.5 g kg^{-1} range. The model stratification resulted in substantial negative buoyancy for this parcel also. Despite these significant differences between the susceptibility of the actual and model soundings to the development of freely convective motions, both soundings were able to realize the potential instability in the 735–685-hPa *layer* with only 1.15 km of lifting. Overall, it is clear that application of the model-based net vertical displacement to the real atmospheric stratification explains the occurrence of a convective component to the snowfall at approximately 1800 UTC. Once again, the model stratification, coupled with a convective parameterization that in the absence of capping inversions does not allow the build up of CAPE, proved to be a compelling factor in the model's underestimate of the snowfall in this case.

5. Post-occlusion forcing of the snowband

As described in Martin (1998), the 19 January cyclone developed a warm-occluded structure around 1800 UTC 19 January. Light to moderate snow continued to fall in Iowa and Wisconsin through 0000 UTC 20 January in association with the warm-occluded structure. In this section, analysis is presented that describes the dynamic and kinematic forcing responsible for the northern third of the snowband, most of which fell in association with the warm occlusion.

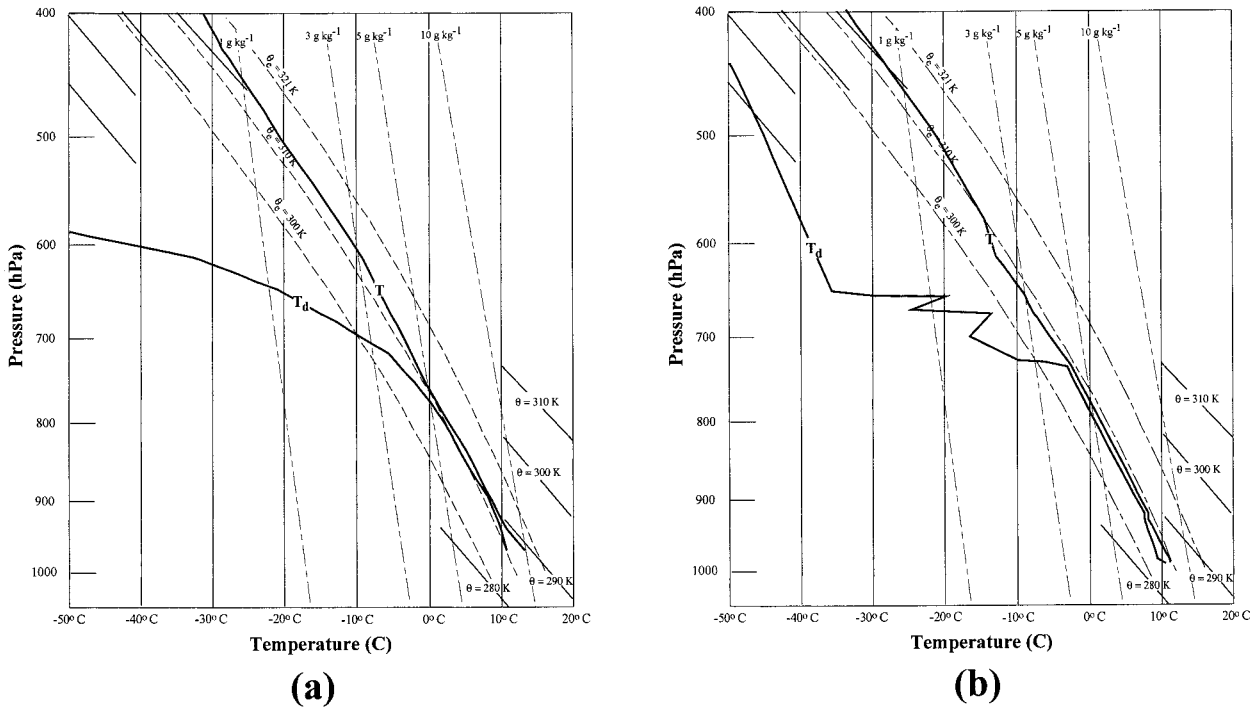

FIG. 14. (a) As in Fig. 10a except UW-NMS 12-h forecast sounding valid at 1200 UTC 19 January 1995 at the unshaded circle in Fig. 13. (b) As in Fig. 10b except observed sounding at Paducah, Kentucky (PAH), at 1200 UTC 19 January 1995.

This will be accomplished with the aid of air parcel trajectories calculated from the gridded model data. A substantial portion of this analysis will center around the concept of the trowal and the previously undiscussed frontal dynamics of the trowal. The next subsection describes some of the characteristics of this feature.

a. The trowal

In the classical Norwegian cyclone model, the warm-occlusion process involved the cold-frontal zone encroaching upon and subsequently ascending the warm-frontal zone. A vertical displacement of original warm sector surface air was presumed to result from such a circumstance. One of the main results of this process was the production of a wedge of warm air aloft displaced poleward of the surface warm-occluded front. In the 1950s, scientists at the Canadian Meteorological Service (Godson 1951; Penner 1955; Galloway 1958, 1960) showed that identification of this trough of warm air aloft (what they termed the trowal) was of great assistance in describing the important characteristics of warm-occluded cyclones. The trowal is a line connecting the crests of the thermal wave at successive heights (Crocker et al. 1947). Godson (1951) referred to a ''sloping valley of tropical air'' in connection with this idea. Galloway (1958), who named the feature, stated that the ''trowal marks the crest of the warm air aloft.'' As such, the trowal marks the 3D sloping intersection of the upper cold-frontal portion of the warm occlusion with the warm-frontal zone. Importantly, the trowal can exist even without an occluded front beneath it (Godson 1951). The motivation for this analysis tool was the observation that the position of this trowal showed a greater correspondence to the cloud and precipitation features associated with an occluded cyclone than did the small wind and temperature changes associated with the warm-occluded front at the surface.

A pair of depictions of the 309-K θ_e surface from the model simulation at 0000 UTC 20 January (Fig. 15) helps to illustrate the nature of the trowal and its place in the warm-occluded structure. Figure 15a shows the topography of the 309-K θ_e surface at 0000 UTC 20 January. The leading edge of the dome of high heights that stretches from central Ohio into northwestern Missouri is the trowal. The dashed line represents the 3D sloping intersection of two different air masses. A 3D perspective of this sloping intersection is afforded in Fig. 15b. The trowal has a fairly continuous slope from $z = 0$ to nearly $z = 6.25$ km. This ''canyon'' in the 309-K θ_e surface provided a narrow causeway through which a warm, moist airstream passed, rising as it did so, generating snow in the northern third of the affected area. We now turn to trajectory analysis to demonstrate this fact.

b. Trajectory analysis of airflow through the trowal

The major lower to middle tropospheric airstreams that characterized this cyclone are shown in Fig. 16. Trajectory A represents the low-level jet that was located on the cold side of the warm-frontal zone. Trajectories B, C, and D are low-level trajectories whose confluence helped to maintain the vigor of the warm-frontal zone throughout the cyclone life cycle. Notice that all three of these trajectories rise upon encountering their confluent point, the rising a result of frontogenesis. Trajectory E describes the warm conveyor belt (i.e., the warm, moist air immediately east of the surface cold front that flows over the warm front) (Harrold 1973; Carlson 1980) of the present case. This trajectory curves slightly anticyclonically over northern Wisconsin during its ascent. Trajectory F is a rising, cyclonically turning trajectory that represents airflow that was largely responsible for the sustenance of the snowband in Iowa and Wisconsin after 1800 UTC 19 January. This airstream describes flow that ascended through the trowal.

As shown by Martin (1998), the trowal can be easily identified in 3D depictions of an appropriate thermodynamic surface. In that paper, the 309-K θ_e surface was chosen to illustrate the 3D morphology of the trowal. Using trajectory F in combination with visualization of the 309-K θ_e surface, an approximate trowal-relative airflow (from 1500 UTC 19 January to 0300 UTC 20 January) was constructed. To portray this trowal-relative flow, the 309-K θ_e surface at 2100 UTC 19 January was used as a representative of the average trowal structure over that time interval. The results of this analysis are shown in Fig. 17. It is clear that trajectory F accomplishes its most rapid ascent (averaging approximately 10 cm s^{-1} over the 12-h interval) in the trowal.[1]

The dynamics and kinematics responsible for this circumstance are, naturally, of interest. The 2D frontogenesis at 1.96 km, at 3-h intervals from 1500 UTC 19 January to 0000 UTC 20 January, is shown in Fig. 18. As trajectories B–F approached the frontogenesis axis, all of them began to rise with E and F rising most dramatically as they experienced the most prolonged and direct exposure to the associated vertical circulation. Importantly, the frontogenesis was associated only with the warm-frontal portion of the developing warm-occluded structure, a point made by Martin (1998).

Trajectory E curved anticyclonically as it rose above the warm front, whereas trajectory F (the trowal trajectory) curved cyclonically as it rose. This fact was of considerable consequence for the snowfall as such cyclonically turning ascent resulted in moderate snowfall to the west and northwest of the surface low pressure

[1] Animation of this ''trowal trajectory'' can be seen at World Wide Web site http://marrella.meteor.wisc.edu/occlusion.html.

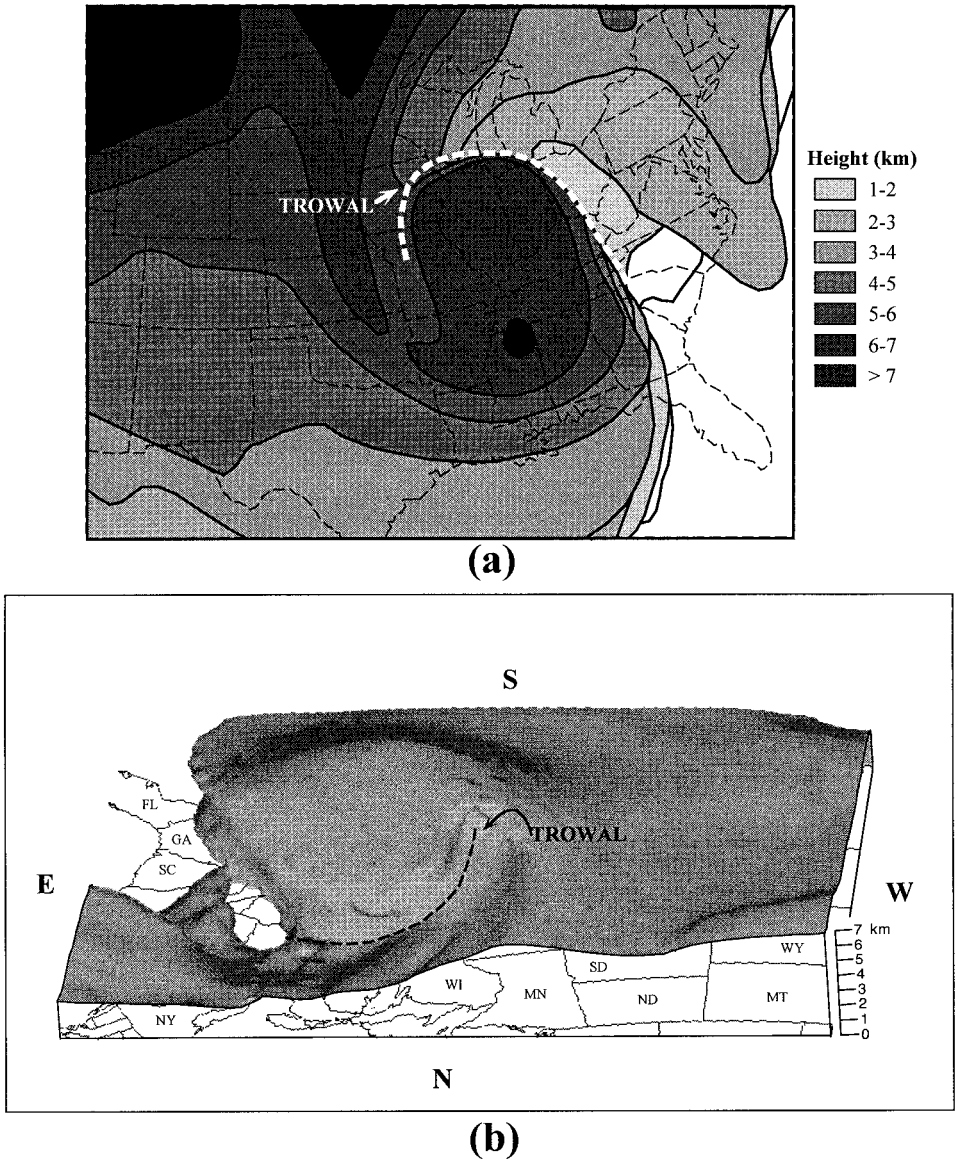

FIG. 15. (a) Plan view of the topography of the 309-K θ_e surface from 24-h forecast from the UW-NMS simulation valid at 0000 UTC 20 January 1995. Thick, white dashed line is the position of the trowal. (b) Elevated, northern perspective of the same 309-K θ_e surface depicted in (a). Dark dashed line is the trowal position, in 3D, at 0000 UTC 20 January 1995.

center. An explanation for this difference is afforded by simple kinematics. In a pure deformation field, the axes of dilatation and contraction delineate four quadrants to the flow field around the col point (Fig. 19a). If rising motion exists on the warm end of the axis of contraction, then quadrant A (B) will be characterized by rising air and anticyclonic (cyclonic) horizontal flow. Trajectory F was consistently located in the rising, cyclonically turning quadrant (Fig. 19b). Trajectory E was located in the rising, anticyclonically turning quadrant after 1800 UTC (not shown). Therefore, the air that ascended the trowal and produced the moderate snowfall in Iowa and Wisconsin did so as a result of frontogenetical lifting into the cyclonically turning quadrant of the upper-level deformation zone.

6. Discussion

Midlatitude cyclones of modest intensity represent the vast majority of all cyclone events (Roebber 1984). Yet the amount of research effort devoted to describing the life cycle and precipitation characteristics of these storms pales in comparison to the volume of work concerned with the relatively rare explosively deepening

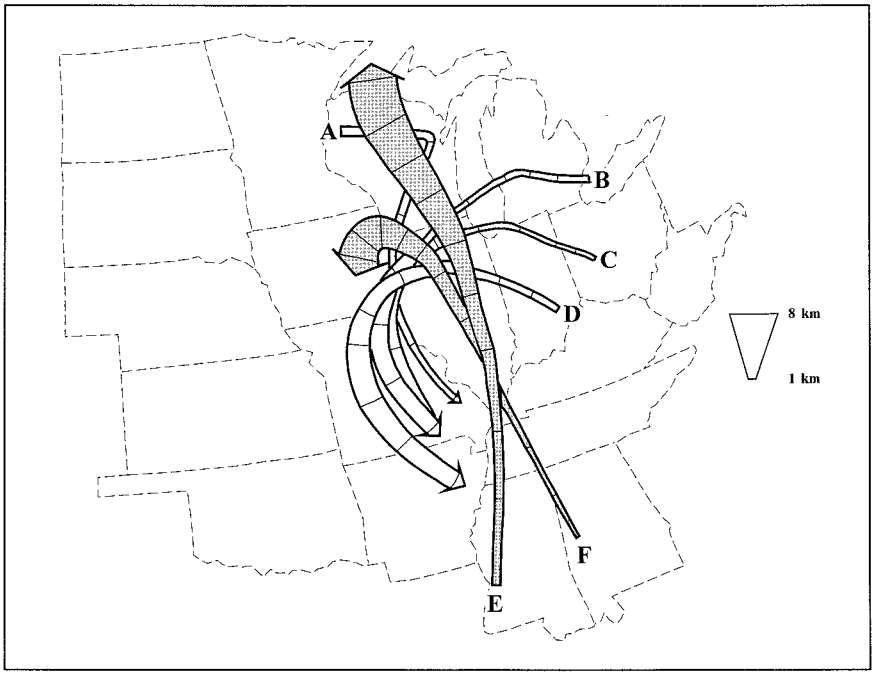

FIG. 16. Absolute trajectories from 0000 UTC 19 January to 0300 UTC 20 January 1995 from the UW-NMS model simulation. See text for explanation of significance. Tick marks on each trajectory represent parcel positions along that trajectory at 3-h intervals. The height of parcels along trajectories is given by the width scale on the right. Trajectories E and F are shaded for ease of illustration only.

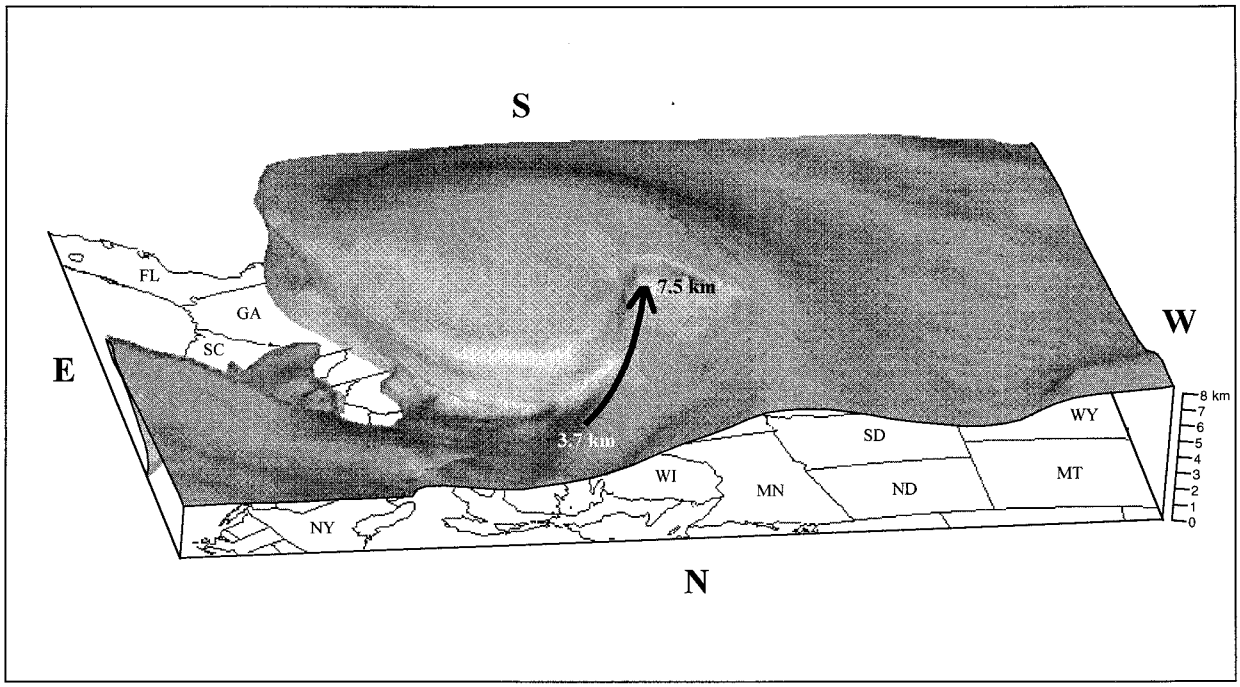

FIG. 17. Heavy solid arrow represents the approximate trowal-relative trajectory from 1500 UTC 19 January to 0300 UTC 20 January 1995. Vertical position at beginning and end of this trajectory is indicated. Constructed with trajectory F in Fig. 16 and using the 2100 UTC 19 January 309-K θ_e surface as representative of the average trowal structure over the time interval.

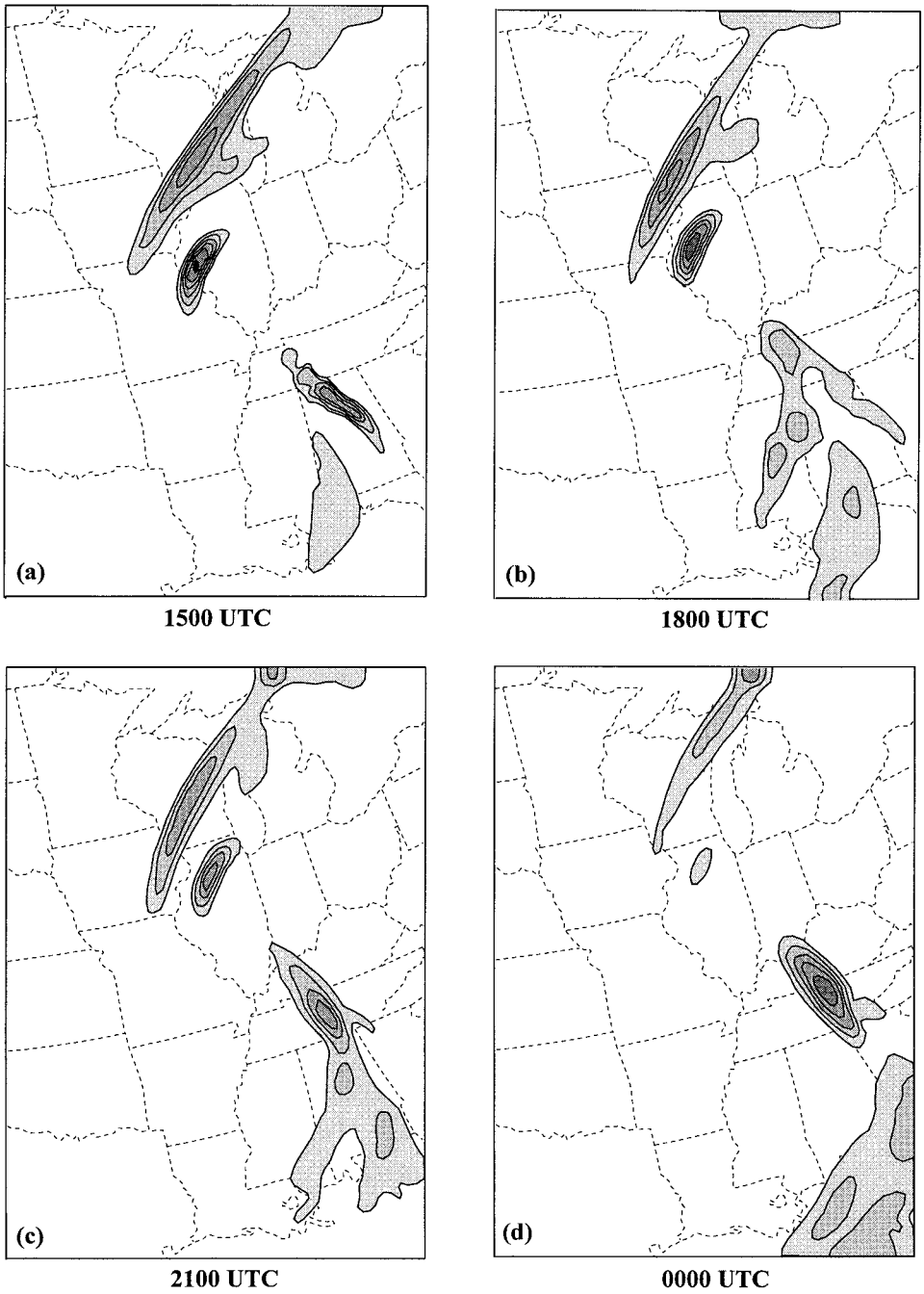

FIG. 18. Two-dimensional frontogenesis function at 1.96 km at (a) 1500 UTC 19 January, (b) 1800 UTC 19 January, (c) 2100 UTC 19 January, and (d) 0000 UTC 20 January 1995. Frontogenesis values are indicated by the same shading as in Fig. 5.

cyclones. Synoptic experience demonstrates an important point made by the present case; modest cyclones can be associated with significant precipitation events because a number of mechanisms in the atmosphere can be responsible for the production of heavy precipitation (i.e., frontogenesis, orographic effects, convection, etc.) but may not simultaneously force systematic surface development. This is particularly likely in the central United States where abundant low-level moisture and a weakly stratified lower troposphere can result in a dramatic response to frontal-scale forcing while the synoptic-scale forcing fails to produce a notable surface disturbance.

In the present case, lower-tropospheric warm fron-

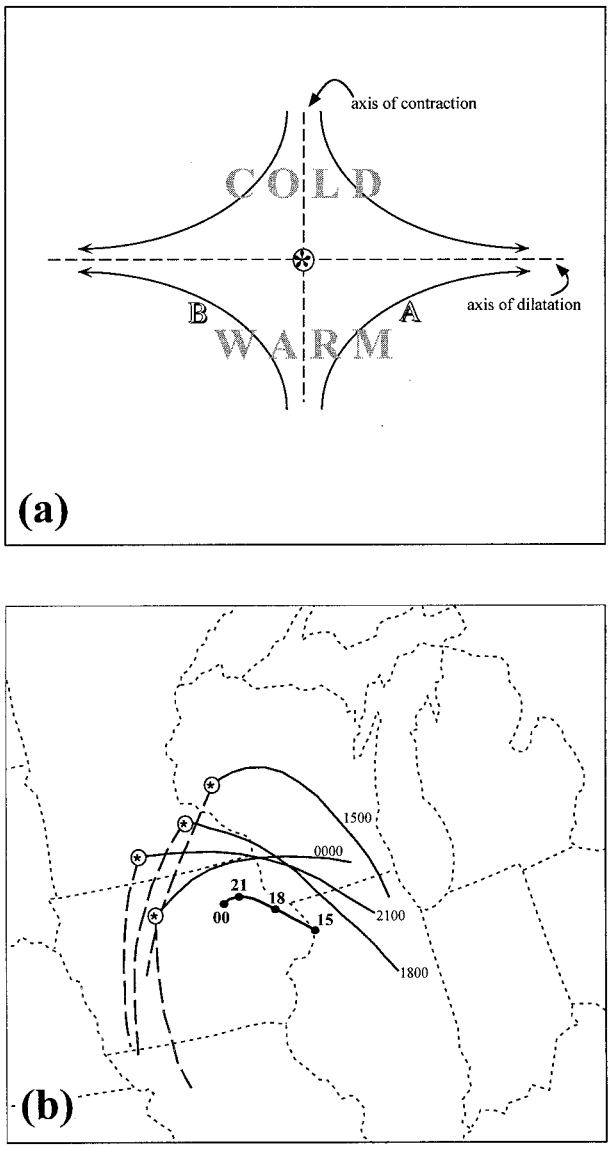

FIG. 19. (a) Schematic of a pure deformation zone. Axes of dilatation and contraction are labeled. Col point indicated by asterisk enclosed in a circle. Warm end of axis of contraction has two quadrants labeled A and B, respectively. Quadrant A (B) is characterized by anticyclonic (cyclonic) horizontal flow. (b) Thick solid line indicates a portion of the path of trajectory F in Fig. 16. Parcel position at 3-h intervals is indicated by 15, 18, 21, and 00. Circled asterisks mark the col point of the deformation field at the trajectory height at each time. Thin solid (dashed) lines emanating from the col point are portions of the axes of contraction (dilatation) at that height and time.

togenesis, and a steady stream of high-θ_e air from the Gulf of Mexico conspired to produce heavy, occasionally convective, snow in the central United States, particularly in central Missouri. The snow fell in narrow bands oriented parallel to the warm front suggesting that a mesoscale instability such as release of CSI may have been a factor in the production of the precipitation. Recent numerical work by Persson and Warner (1993) has suggested that CSI circulations (and, by extension, the structures associated with them) cannot be explicitly resolved in models with horizontal grid spacing coarser than 30 km. The present study employed a 40-km horizontal grid spacing and therefore no definitive statement concerning the presence or absence of CSI in this case can be made. However, the model atmosphere was assessed for regions in which the necessary condition for CSI was met. It was found that saturated regions of CSI did not appear in the simulated frontal environment suggesting it may not have been an important factor. Instead, frontogenesis in the presence of across-front differences in the effective static stability (as measured in terms of PV_e) was found to be the circumstance responsible for the intensity and dimensions of the snowband. It was determined that release of convective instability in the ascending branch of the thermally direct frontal circulation provided the convective component to the band, manifested in cloud-to-ground lightning and occasional bursts of 5 cm h^{-1} snowfall rates. The double-banded structure exhibited in Fig. 6 may have been the result of releases of multiple regions of convective instability in the frontal updraft. More detailed observations are required to determine the viability of this hypothesis.

The existence of ''wrap around'' precipitation in occluded cyclones has long been recognized by operational forecasters and can take the form of prolonged, heavy snow in winter-occluded systems. In Canada, the concept of the trowal has proven useful in the analysis of such storms for the past 45 years. The present case demonstrates that the trowal is a dynamically significant component of a warm-occluded frontal structure and, as such, is involved in the production of this so-called wrap-around precipitation. Currently, case studies are being collected that document the synoptic-scale dynamics of the trowal in order to place this useful conceptual model in its proper dynamical context.

7. Conclusions

On 19 January 1995 a modest cyclone affected the central United States. This cyclone was attended by an 1100-km-long narrow band of heavy snow that was accompanied by thunder and lightning, heavy winds, and record breaking snowfall totals. The snowband was forced by the vertical circulation associated with lower-tropospheric warm frontogenesis that was continually supplied with high-θ_e, Gulf of Mexico air throughout the lifetime of the cyclone. The narrow cross-band width and the intensity of the vertical motions that forced the band were found to result from frontogenesis in the presence of across-front differences in effective static stability, as predicted by theory. Although the band exhibited characteristics that suggested release of CSI may have played a role in

its formation, the model resolution used here was too coarse to confirm or deny its operation in this case. Significantly, however, no evidence of saturated regions of CSI in the model-simulated frontal environment were found. The convective nature of the snowband was accounted for by the development of free convection forced by frontal lifting of the observed environmental stratification.

Ascent of warm, moist air in the trowal portion of the warm-occluded structure that developed in this case was shown to contribute to the heavy snowfall. Frontogenesis along the warm-frontal portion of the warm-occluded structure forced the lifting of air into and through the trowal. It is suggested that the trowal, which was a focus of frontogenesis to the northwest of the cyclone center in this case, is easily identifiable given emerging visualization technologies. It is anticipated that such technologies may reinvest some of these older conceptual ideas with a new, practical relevance in the short term forecasting of prolonged snow events as well as contribute to greater understanding of precipitation production in extratropical cyclones.

Acknowledgments. The author would like to thank Dr. Greg Tripoli and Peter Pokrandt for their willing and able NMS model expertise. Sebastien Korner assisted with many of the numerical model runs. Thanks also to Dr. Michael Morgan and Kevin Coskren for helpful discussions concerning this work. Satellite data were provided by Dr. Phillip J. Smith and Mr. Dan Vietor at Purdue University. This research was supported by the National Science Foundation under Grant ATM-9505849.

REFERENCES

Bennetts, D. A., and B. J. Hoskins, 1979: Conditional symmetric instability—A possible explanation for frontal rainbands. *Quart. J. Roy. Meteor. Soc.*, **105,** 945–962.

Carlson, T. N., 1980: Airflow through midlatitude cyclones and the comma cloud pattern. *Mon. Wea. Rev.,* **108,** 1498–1509.

Chen, C., and W. R. Cotton, 1983: A one-dimensional simulation of the stratocumulus capped mixed layer. *Bound.-Layer Meteor.,* **25,** 289–321.

Cotton, W. R., G. J. Tripoli, R. M. Rauber, and E. A. Mulvihill, 1986: Numerical simulation of the effects of varying ice crystal nucleation rates and aggregation processes on orographic snowfall. *J. Climate Appl. Meteor.,* **25,** 1658–1680.

Crocker, A. M., W. L. Godson, and C. M. Penner, 1947: Frontal contour charts. *J. Meteor.,* **4,** 95–99.

Dunn, L. B., 1988: Vertical motion evaluation of a Colorado snowstorm from a synoptician's perspective. *Wea. Forecasting,* **3,** 261–272.

Eliassen, A., 1962: On the vertical circulation in frontal zones. *Geofys. Publ.,* **24,** 147–160.

Emanuel, K. A., 1983: Lagrangian parcel dynamics of moist symmetric instability. *J. Atmos. Sci.,* **40,** 2368–2376.

——, 1991: A scheme for representing cumulus convection in large-scale models. *J. Atmos. Sci.,* **48,** 2313–2335.

Flatau, P., G. J. Tripoli, J. Verlinde, and W. R. Cotton, 1989: The CSU RAMS cloud microphysical module: General theory and code documentation. Tech. Rep. 451, Dept. of Atmos. Sci., Colorado State University, 88 pp. [Available from Dept. of Atmos. Sci., CSU, Fort Collins, CO 80523.]

Funk, T. W., C. W. Hayes, M. B. Scholz, and K. A. Kostura, 1995: Vertical motion forcing mechanisms responsible for the production of a mesoscale very heavy snow band. Preprints, *14th Conf. on Weather Analysis and Forecasting,* Dallas, TX, Amer. Meteor. Soc., 176–181.

Galloway, J. L., 1958: The three-front model: Its philosophy, nature, construction and use. *Weather,* **13,** 3–10.

——, 1960: The three-front model, the developing depression and the occluding process. *Weather,* **15,** 293–301.

Godson, W. L., 1951: Synoptic properties of frontal surfaces. *Quart. J. Roy. Meteor. Soc.,* **77,** 633–653.

Gyakum, J. R., 1987: Evolution of a surprise snowfall in the United States midwest. *Mon. Wea. Rev.,* **115,** 2322–2345.

Hakim, G. J., and L. W. Uccellini, 1992: Diagnosing coupled jet-streak circulations for a northern plains snowband from the operational Nested Grid Model. *Wea. Forecasting,* **7,** 26–48.

——, L. F. Bosart, and D. Keyser, 1995: The Ohio Valley wave-merger cyclogenesis event of 25–26 January 1978. Part I: Multiscale case study. *Mon. Wea. Rev.,* **123,** 2663–2692.

Harrold, T. W., 1973: Mechanisms influencing the distribution of precipitation within baroclinic disturbances. *Quart. J. Roy. Meteor. Soc.,* **99,** 232–251.

Hoskins, B. J., I. Draghici, and H. C. Davies, 1978: A new look at the ω-equation. *Quart. J. Roy. Meteor. Soc.,* **104,** 31–38.

Martin, J. E., 1998: The structure and evolution of a continental winter cyclone. Part I: Frontal structure and the occlusion process. *Mon. Wea. Rev.,* **126,** 303–328.

——, J. D. Locatelli, and P. V. Hobbs, 1992: Organization and structure of clouds and precipitation on the mid-Atlantic coast of the United States. Part V: The role of an upper-level front in the generation of a rainband. *J. Atmos. Sci.,* **49,** 1293–1303.

Marwitz, J., and J. Toth, 1993: A case study of heavy snowfall in Oklahoma. *Mon. Wea. Rev.,* **121,** 648–660.

Mass, C. F., and D. M. Schultz, 1993: The structure and evolution of a simulated midlatitude cyclone over land. *Mon. Wea. Rev.,* **121,** 105–117.

McCann, D. W., 1995: Three-dimensional computations of equivalent potential vorticity. *Wea. Forecasting,* **10,** 798–802.

Miller, J. E., 1948: On the concept of frontogenesis. *J. Meteor.,* **5,** 169–171.

Moore, J. T., and P. D. Blakely, 1988: The role of frontogenetical forcing and conditional symmetric instability in the Midwest snowstorm of 30–31 January 1982. *Mon. Wea. Rev.,* **116,** 2155–2171.

——, and T. E. Lambert, 1993: The use of equivalent potential vorticity to diagnose regions of conditional symmetric instability. *Wea. Forecasting,* **8,** 310–308.

Penner, C. M., 1955: A three-front model for synoptic analyses. *Quart. J. Roy. Meteor. Soc.,* **81,** 89–91.

Persson, P. O. G., and T. T. Warner, 1993: Nonlinear hydrostatic conditional symmetric instability: Implications for numerical weather prediction. *Mon. Wea. Rev.,* **121,** 1821–1833.

Petterssen, S., 1936: Contribution to the theory of frontogenesis. *Geofys. Publ.,* **11**(6), 127.

Roebber, P. J., 1984: Statistical analysis and updated climatology of explosive cyclones. *Mon. Wea. Rev.,* **112,** 1577–1589.

Sadourny, R., 1975: The dynamics of finite-difference models of shallow water equations. *J. Atmos. Sci.,* **32,** 680–689.

Sanders, F., 1986: Frontogenesis and symmetric stability in a major New England snowstorm. *Mon. Wea. Rev.,* **114,** 1847–1862.

——, and L. F. Bosart, 1985: Mesoscale structure in the megalopolitan snowstorm of 11–12 February 1983. Part I: Frontogenetical forcing and symmetric instability. *J Atmos. Sci.,* **42,** 1050–1061.

Sawyer, J. S., 1956: The vertical circulation at meteorological

fronts and its relation to frontogenesis. *Proc. Roy. Soc. London,* **A234,** 346–362.

Schneider, R. S., 1990: Large-amplitude mesoscale wave disturbances within the intense Midwest extratropical cyclone of 15 December 1987. *Wea. Forecasting,* **5,** 533–558.

Shea, T. J., and R. W. Przybylinski, 1993: Assessing vertical motion fields in a winter storm using PCGRIDDS. Preprints, *13th Conf. on Weather Analysis and Forecasting,* Vienna, VA, Amer. Meteor. Soc., 10–14.

Shields, M. T., R. M. Rauber, and M. K. Ramamurthy, 1991: Dynamical forcing and mesoscale organization of precipitation bands in a Midwest winter cyclonic storm. *Mon. Wea. Rev.*, **119,** 936–964.

Thorpe, A. J., and K. A. Emanuel, 1985: Frontogenesis in the presence of small stability to slantwise convection. *J. Atmos. Sci.,* **42,** 1809–1824.

Trembach, C. J., and R. Kessler, 1985: A surface temperature and moisture parameterization for use in mesoscale numerical models. Preprints, *Seventh Conf. on Numerical Weather Prediction,* Montreal, PQ, Canada, Amer. Meteor. Soc., 355–358.

——, J. Powell, W. R. Cotton, and R. A. Pielke, 1987: The forward-in-time upstream advection scheme: Extension to higher orders. *Mon. Wea. Rev.,* **115,** 540–555.

Tripoli, G. J., 1992a: An explicit three-dimensional nonhydrostatic numerical simulation of a tropical cyclone. *Meteor. Atmos. Phys.,* **49,** 229–254.

——, 1992b: A nonhydrostatic numerical model designed to simulate scale interaction. *Mon. Wea. Rev.,* **120,** 1342–1359.